Environ Monit Assess (2011) 183:409–423
DOI 10.1007/s10661-011-1929-6

Detection and object-based classification of offshore oil slicks using ENVISAT-ASAR images

Sertac Akar · Mehmet Lutfi Süzen · Nuretdin Kaymakci

Received: 26 August 2010 / Accepted: 8 February 2011 / Published online: 8 March 2011

Abstract The aim of this study is to propose and test a multi-level methodology for detection of oil slicks in ENVISAT Advanced Synthetic Aperture Radar (ASAR) imagery, which can be used to support the identification of hydrocarbon seeps. We selected Andrusov Ridge in the Central Black Sea as the test study area where extensive hydrocarbon seepages were known to occur continuously. Hydrocarbon seepage from tectonic or stratigraphic origin at the sea floor causes oily gas plumes to rise up to the sea surface and form thin oil films called oil slicks. Microwave sensors like synthetic aperture radar (SAR) are very suitable for ocean remote sensing as they measure the backscattered radiation from the surface and show the roughness of the terrain. Oil slicks dampen the sea waves creating dark patches in the SAR image. The proposed and applied methodology includes three levels: visual interpretation, image filtering and object-based oil spill detection. Level I, after data preparation with visual interpretation, includes dark spots identification and subsets/scenes creation. After this process, the procedure continues with categorization of subsets/scenes into three cases based on contrast difference of dark spots to the surroundings. In level II, by image and morphological filtering, it includes preparation of subsets/scenes for segmentation. Level III includes segmentation and feature extraction which is followed by object-based classification. The object-based classification is applied with the fuzzy membership functions defined by extracted features of ASAR subsets/scenes, where the parameters of the detection algorithms are tuned specifically for each case group. As a result, oil slicks are discriminated from look-alikes with an overall classification accuracy of 83% for oil slicks and 77% for look-alikes obtained by averaging three different cases.

Keywords Synthetic aperture radar (SAR) · Oil slick · Object-based classification · Black Sea

S. Akar · M. L. Süzen (✉) · N. Kaymakci
Geological Engineering Department,
Middle East Technical University,
Inonu Bulvari 06531 Ankara, Turkey
e-mail: suzen@metu.edu.tr

Introduction

Oil slicks on sea surface can have different sources such as manmade slicks from illegal discharges of ships or spill resulting from ship accidents, slicks originated from biological activities such as photo-oxidation processes or by planktons, and geological slicks originated as of natural hydrocarbon seeps from a reservoir. Including every kind of slicks, 10% of ocean surface is estimated to be covered by slicks (Girard-Ardhuin et al. 2003). Natural seepage detection is considered to be one of

the significant preliminary works for offshore petroleum exploration. However, it does not explain the whole petroleum system by itself, and it should be combined with regular exploration techniques such as seismic interpretation, sample collection from sea bottom, and geological survey. The oil slick detection and mapping is becoming one of the standard tools for hydrocarbon exploration activities and has been applied to most of the hydrocarbon basins in the world such as Gulf of Mexico (Friedman et al. 2002), Santa Barbara Channel, California (Leifer et al. 2006), Australian Shelf (O'Brein et al. 2005), and South Caspian Sea (Williams and Lawrence 2002). Black Sea basin is one of the last under-explored basins in the world with very high hydrocarbon potential. In this context, the central part of the Black Sea basin is selected as test area for application of SAR remote sensing techniques for the detection of oil slicks.

Microwave sensors are the most applicable tools for oil slick monitoring since they are not affected by clouds, haze, weather conditions, and day/night differences. Synthetic aperture radar (SAR) is the most common method to detect offshore oil slicks. Parameters used to detect oil slicks are functions of radar configuration, slick nature, meteorological and oceanic conditions like height of the waves, the amount of oil that has been released, and the speed of the wind (Espedal and Wahl 1999; Girard-Ardhuin et al. 2003).

Radar image is a representation of the backscatter electromagnetic pulse, which is also called "echo," from the surface and the intensity of the pixel, which is proportional to the surface roughness at the scale of Bragg scattering (Allan 1983; Ryerson 1998). Since the image brightness is a reflection of the microwave backscattering properties of the surface, it can be used to map natural and anthropogenic oil slicks via the dampening effect of the liquid hydrocarbons. Radar backscattering level is decreased with slick, which appears as a dark patch with lower backscatter from the sea surface because of "Bragg scattering" compared to surroundings of the patch in a radar image (Girard-Ardhuin et al. 2003).

The biggest difficulty that makes oil slick detection from SAR images challenging is the discrimination of look-alikes from oil slicks. Look-alikes are the manifestations that are produced by oceanic and atmospheric processes which yield as dark patches in SAR images similar to oil slicks. Look-alikes include natural organic films, grease ice, swirls, rain cells, and low wind speed areas of less than 3 m/s (Hovland et al. 1994; Solberg et al. 1999, 2007). Discriminative features of oil slicks and look-alikes are basically geometrical, radiometric, textural, and temporal features (Brekke and Solberg 2005; Karantzalos and Argialas 2008; Topouzelis 2008). Natural oil slicks originated from subsurface should be permanent, and temporally many different slicks should be present in a close neighborhood with repetitive manner. However, orientation, shape, and texture can be different because of the weather conditions at the time of image acquisition (Karathanassi et al. 2006; Topouzelis 2008). In this contribution, we aimed at proposing a multi-level methodology for detection of oil slicks using ENVISAT Advanced Synthetic Aperture Radar (ASAR) imagery, which can be used to support the identification of hydrocarbon seeps, and to present our result from Central Black Sea.

Background

Hydrocarbon seepage and oil slick

Hydrocarbon seepage is the surface expression of a migration pathway, along which petroleum is currently flowing through water-wet pores and fractures, driven by buoyancy from a sub-surface origin (Clarke and Cleverly 1991; Rollet et al. 2006). Formation of hydrocarbon seeps at the seafloor can be due to various factors either tectonic (fault systems, mud volcanoes) or stratigraphic origin (Macdonald et al. 2002). The amount of seepage is potentially related to the pressure in oil and gas reservoirs, which in turn is related to hydrostatic pressure and changes in lithospheric stress (Rollet et al. 2006).

The seeping oil and gas are typically considered to rise rapidly to the surface and are often transported as thin slicks on the surface of gas

bubbles, known as "oil pancakes" typically 0.5 to 1 m in diameter (Macdonald et al. 2002; O'Brein et al. 2005). These bubbles have been shown to rise at speeds exceeding those of ocean currents, and hence, seepage slicks are typically developed initially on the sea's surface no further away from the seafloor seepage vent than a distance roughly equivalent to the water depth.

Offshore oil slicks are highly time-depended structures and require a detailed survey of comparison of individual seep activities over time. Crude oil on the sea surface undergoes some physical and chemical changes affecting their distribution and temporal existence including various processes of weathering like spreading, evaporation, dispersion, emulsification, dissolution, oxidation, sedimentation, and biodegradation (Pellemans et al. 1995; Dalling and Strøm 1999; Nirchio et al. 2005). Oil detection depends on the local weather conditions that determine its fate on the water's surface (Nirchio et al. 2005). Some slicks are observed to be perennial since they are produced approximately in the same location in multiple images. The weather conditions especially the wind speed and the wind direction cause this variation in the location of the oil slicks. Heavier (low API) oils are the easiest to detect because they have longer residence times at the sea surface, whereas condensates and light oils evaporate much more rapidly (O'Brein et al. 2005).

Literature review on oil slick detection

Immense literature has already been accumulated about oil slick detection over the last two decades after satellite SAR images become publicly available. One of the well-known studies made by Solberg et al. (1999) consists of applying an adaptive threshold to the image for dark spot detection, feature extraction, and slick classification stages. Some of the filtering techniques that have been used in literature were cross-spectral phase filtering (Smith and Melger 2003), Bayesian approach speckle filtering (Arvelyna et al. 2001), and Lee filtering (Karathanassi et al. 2006). In addition to these, statistical approaches have been applied to classify slicks and differentiate look-alikes. For instance, fractionally integrated autoregressive-moving average has been used to discriminate the oil slicks from low wind areas (Bertacca et al. 2005); a probabilistic approach to distinguish oil spills from other similar oceanic features has also been developed (Fiscella et al. 2000).

One of the most marginal methods is to compare different polarization measures applied to the detection of slicks to define their boundaries. Annealed segmentation of these measures is employed to detect and define their boundaries including the intensity in a single polarization and the maximum eigenvalue and span measures for more than one polarization channel (Lombardo and Oliver 2000). Segmentation is also one of the most frequently used methods (Brekke and Solberg 2005; Karantzalos and Argialas 2008; Shu et al. 2010; Li and Shen 2010). Segmentation of oil slicks using a partial differential equation-based level set method, which represents the slick surface as an implicit propagation interface, is one of the approaches (Huang et al. 2005), where another one is auto-segmentation with co-occurrence techniques (Arvelyna et al. 2001). Object-based fuzzy classification is used as a continuation of segmentation and an alternative to probabilistic approaches for slick classification (Keramitsoglou et al. 2006).

Study area: Central Black Sea

The Black Sea is a semi-enclosed sea located between 40°55′ to 46°32′ N and 27°27′ to 41°32′ E, whose only connection to the worlds' oceans is the narrow Bosphorus Strait. Total area is 436,400 km^2 with maximum and average depths of 2,200 and 1,240 m, respectively. The study area is just located just above the Andrusov ridge located at the center of the basin. Andrusov ridge, together with the Archangelski ridge, separates the Black Sea Basin into two sectors as the western and the eastern Black Sea basins (Fig. 1).

Black Sea is one of the frontier basins in the world in having high hydrocarbon potential especially within the thick Neogene deposits accumulated due to drainage of many of the major

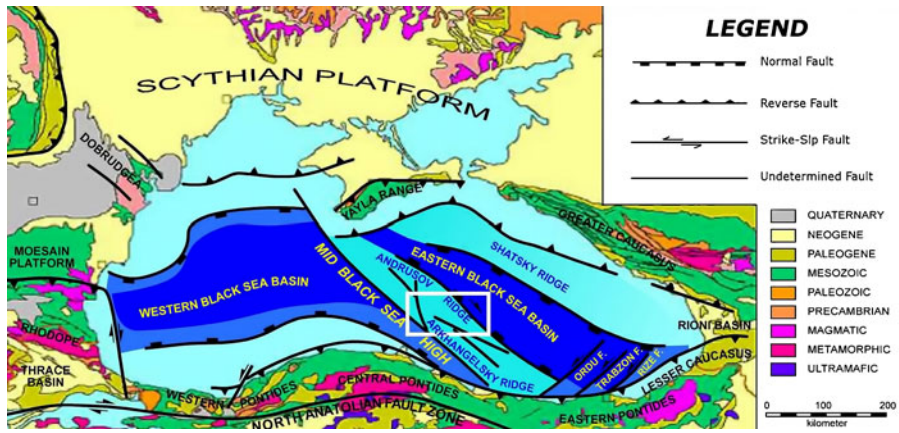

Fig. 1 Location map of the study area (modified from Okay et al. 1994)

rivers of Eurasia into basin (Roberts 1998). There are several potential fields for the oil and operational ones for gas generation throughout the basin. These generally anticlines and extensional structures in Gulf of Odessa (Robinson et al. 1996), mud volcano area in the deep waters southeast of the Crimean Peninsula (Greinert et al. 2006), foreland extensional structures of Bulgarian waters and Romanian shelf (Robinson et al. 1996), Central Azov High around the Sea of Azov, Shatsky Ridge offshore Russia and Georgia, compressional structures of the northern Turkish coast (Ergün et al. 2002), and the extensional fault blocks of the Andrusov Ridge (our study area) are the examples considered to have high hydrocarbon potential (Robinson et al. 1996).

Satellite configuration and input data

Satellite configuration is the starting point for the oil slick detection procedure. There are a number of different SAR missions available for radar remote sensing and with different configurations for polarization, spectral and spatial resolutions. Several experimental studies with multi-frequencies consisting of tipping artificial slicks have shown most important contrast with C-, X-, and Ku-bands with 5 dB contrast for a slick made with "light" fuel and 10 to 15 dB contrasts for a "heavy" fuel. Moreover, L- and S-bands are weakly affected by slicks (Girard-Ardhuin et al. 2003). Furthermore, in the literature for oil slick detection VV polarized, C-band with low incidence angle data is considered preferable (Fingas and Brown 1997; Girard-Ardhuin et al. 2003, 2005; Brekke and Solberg 2005; Mouche et al. 2005). In this study, image mode, VV polarization, level 1b ASA_IMP_1P, and swath IS2 (105 km width and incidence angle 19.2–26.7) are used.

The study area is covered by four different ENVISAT-ASAR scenes where three of them also have three multitemporal images acquired during summer 2004, spring 2005, and summer 2005, yielding in a total number of ten images. Total area is a rectangle of 220 × 160 km (excluding the overlapping regions of the images). The details of data set containing the information about date, time, orbit, track, and frame are given in Table 1.

Table 1 ENVISAT-ASAR input dataset information

ENVISAT-ASAR input data set			
Date	Time	Orbit	Frame
07 August 2004	07:55:33	12,743	2,745
23 August 2004	07:52:39	12,972	2,745
23 August 2004	07:52:24	12,972	2,727
23 July 2005	07:55:35	17,753	2,745
08 August 2005	07:52:39	17,982	2,745
08 August 2005	07:52:24	17,982	2,727
14 May 2005	07:55:34	16,751	2,745
14 May 2005	07:55:20	16,751	2,727
25 April 2005	07:52:25	16,479	2,745
25 April 2005	07:52:42	16,479	2,727

Methodology

The methodology in this study is an implementation of pre-existing techniques, with a new

approach, to three differing contextual levels: two for dark spot detection and one for dark spot classification (Fig. 2). The first level comprises visual interpretation composed of visual interpretation of images and creation of subsets based on the locations of dark objects. The second level includes the image processing and filtering operations. The third level is the object-based oil spill detection stage, which includes segmentation, feature extraction, and object-based classification.

Level I: visual interpretation

Visual interpretation starts with a pre-processing stage where artifacts (if applicable) resulting in different contrast trends across the images (range falloff, gain control effects, etc.) have been determined and removed (Wackerman 1992). The de-trended images with balanced contrast have been scanned visually to determine the target dark spots. The human eye is superior in observing a

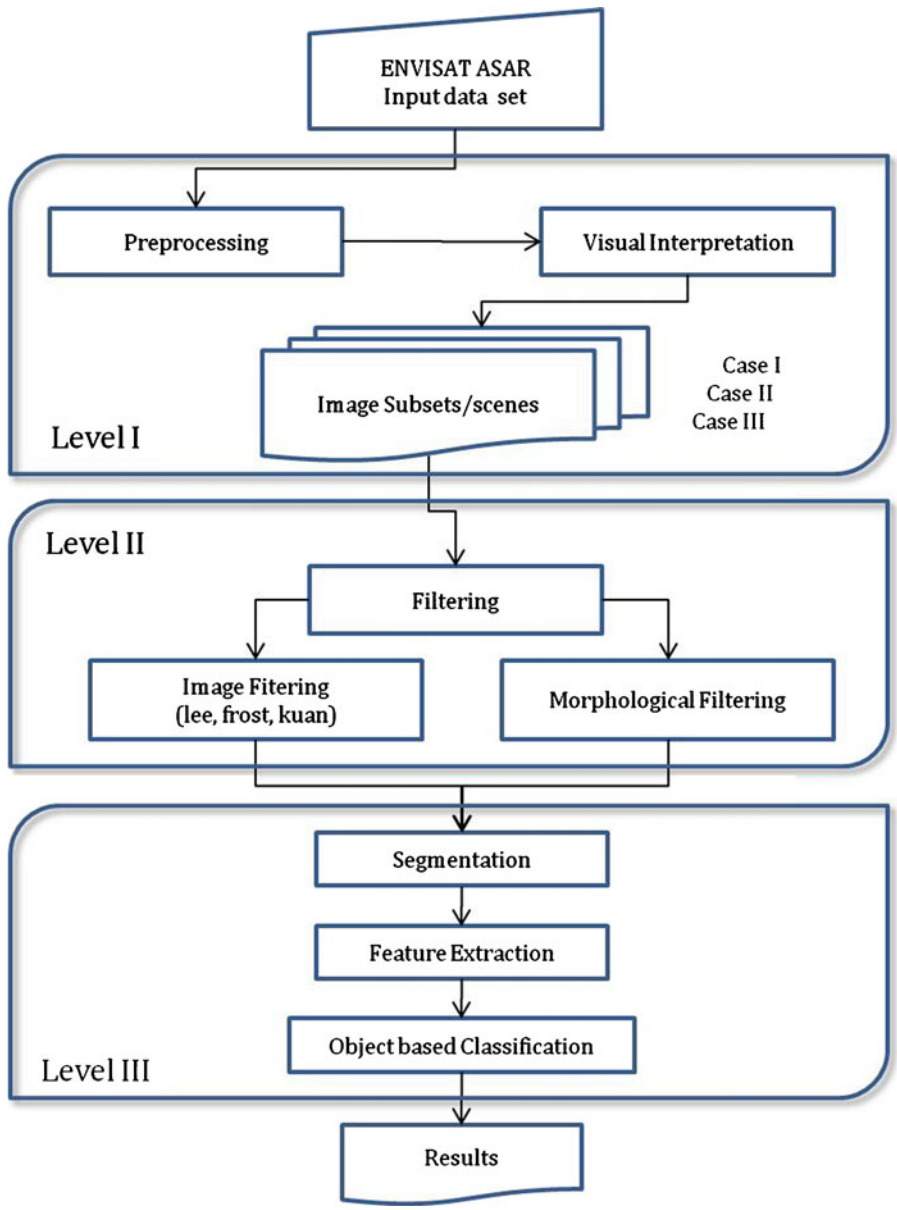

Fig. 2 Flowchart of the methodology

slick in the context of the surrounding sea, and a trained human interpreter can discriminate oil slicks and look-alikes based on experience and a priori information concerning location, external information about weather conditions, differences in shape, and contrast to surroundings between oil slicks and look-alikes (Solberg et al. 1999; Fiscella et al. 2000). If the surroundings are homogeneous, the human observer will have more belief in that the spot is an oil slick than with heterogeneous surroundings (Solberg et al. 1999). With heterogeneous surroundings, the human eye can easily determine if the spot is separated from the surroundings based on contrast or orientation.

In this study, the subset images are extracted based on target areas containing dark spots on the bases of contrast level to the surroundings, homogeneity of the surroundings, wind patterns, nearby bright spots of ships, edge, and shape characteristics for natural slicks. Closely spaced, a number of dark spot groups or large individual ones are limiting the subsets spatially. The subsets and later scenes (parts of subsets) have been created to speed up the processes and to fine tune the parameters of segmentation and classification algorithms.

Level II: image filtering

Image filtering level aims to reduce speckle and to enhance the image. This level consists of two stages: One is the filtering of image with noise removal filters like Lee, Frost, or Kuan filters, where the other branch is morphological filtering to emphasize morphology of the dark spots in the image. In terms of minimum loss of textural information and preserving edges, filtering operations with 3×3 kernels are considered to give better results (Rudorff and Gherardi 2008).

Filtering of the image with noise removal filters gives a clear output for discrimination of dark areas from the remaining heterogeneous background. The type of applied algorithms is not so vital because all of the three filters aim to remove noise without altering the characteristics of the edges and sharp features. During the second stage, morphological filtering is utilized based on geometry and the shapes within images in its processes. The morphology filters requires the data to be coded in 8-bit integer coding; hence, the 32-bit floating point pixel values of SAR images are rescaled down to 8 bit, assigning the minimum and the maximum values to 0 and 255, respectively. Morphological transformation simplifies the image and enhances object structure, while maintaining the primary shape characteristics within the object. Most common morphological functions are "dilation," which fills the holes smaller than the structural element, and "erosion," which does the reverse of dilate function (Gonzalez and Richards 1992; Russ 1992). In addition to this, there are also "opening" (erosion followed by dilation) and "closing" ("dilation" followed by "erosion") functions which are useful for dark spot detection. In this study, the "opening" and "closing" morphology operators are used.

Level III: object-based oil spill detection

Segmentation

In the literature, a number of segmentation procedures are available for solving different problems. Among the frequently used algorithms, Meinel and Neubert (2004) proposed an application-oriented quality test and reported that region growing-based algorithms yield the best results. The best method is based on "fractal net evolution algorithm" (FNEA) approach which is an efficient method to describe semantics within largely self-constructing and dynamic networks. It combines fractal structure of the world and semantics with object orientation (Baatz and Schäpe 2000). FNEA is already embedded in a commercial software "eCognition" of Definiens Inc.

The first process of this stage is segmentation which allows knowledge free extraction of homogeneous image object primitives in any chosen resolution, especially taking into consideration local contrasts. Generally throughout different types of texture segmentation algorithms, the modeling and the optimization stages have been followed (Haralick et al. 1973; Mao and Jain 1992; Hofmann et al. 1998). In the modeling stage, characteristic features are extracted from the textured input image and range from spatial frequencies and co-occurrence matrices to wavelet coefficients, wave

packets, and fractal indices. In the optimization stage, features are grouped into homogeneous segments by minimizing an appropriate quality measure. This is most often achieved by a few types of clustering cost functions.

In this study, two input layers are used for the segmentation. The first layer is the filtered subset image, and the second layer is the result of morphological filter. Different weight parameters are assigned for input layers depending on their importance or suitability for the segmentation result. Higher weight has been given to the layer from which more information will be used during the segmentation process. Segmentation may also be done from one layer, but better results can be achieved if more than one layer is used (eCognition 2004).

The segmentation is generated based upon several adjustable criteria, like shape factor, scale parameter, smoothness, and compactness. The scale parameter determines the size of the resulting image objects. In this study, larger-scale parameter is used for heterogeneous subset scenes, and conversely, smaller-scale parameter is used for homogeneous subset scenes. The shape factor helps to avoid fractal shaping of objects in strongly textured radar data and improves quality of object extraction. The smoothness criterion optimizes image objects with regard to smooth borders and is a very important parameter when working on very heterogeneous radar images in order to maintain non-compact objects. The compactness criterion is inversely related to smoothness and used to optimize image objects with regard to compactness to identify object with relatively weak contrast. A strong and experienced means for the evaluation of segmentation techniques is the human eye; hence, the results of the segmentation are supervised until representative segments of dark spots are achieved.

Feature extraction

After segments have been created, features related to "layer values," "shape," and "texture" are computed for each segment. Important features related to layer values (intensity value of an image) are mean layer value, mean brightness value, minimum and maximum pixel values, mean difference to neighbor pixels, and mean difference to scene. Features related to shape are area, length to width ratio, compactness, and shape index. Features related to texture are homogeneity, contrast, and dissimilarity. These features are used for defining the boundaries of the membership functions while making object-based fuzzy classification.

Membership functions

The last stage includes defining membership functions based on extracted object features. An object-based fuzzy classification scheme is used for discriminating dark spots, with a simple empirical class hierarchy consisting of two classes which are "clear sea water" and "dark spots." "Dark spots" class includes two subclasses, namely "probable oil slicks" and "probable look-alikes."

Fuzzification describes the transition from a crisp system to a fuzzy system. Fuzzy rule can have a single condition or can consist of a combination of conditions that have to be fulfilled for a dark object to be assigned to a probability class (Karathanassi et al. 2006). Membership function assigns a membership degree or value between 0 and 1 to each feature. Boundaries of membership functions are determined based on feature value intervals from randomly selected representative segments that are supposed to belong to a specific class. In most of the cases, "Boolean range function" is used, which assigns a value of "1" between specific values and assigns "0" for the rest, in order to achieve sharp distinction of "probable oil slick" and "probable look-alike" classes.

For successful classification, a deliberate choice of membership function is crucial. This allows the introduction of expert knowledge into the system. The better the knowledge about the real system is modeled by the membership functions, the better the final classification will result. In fuzzy classification methods, segments whose feature values are within these overlapping ranges can be seen as ambiguous objects and can belong to more than one class but with different degrees of membership (eCognition 2004). Although it is possible to reassign these ambiguities to a class by their degree of likelihood, the main aim is to define classes as unambiguously as possible.

Table 2 Category description for the three different cases of dark spot occurrences

Categories	Number of subscenes	Category description	
		Dark spot orientation	Contrast to surroundings
Case 1	6	Multi-directional	Moderate
Case 2	11	Uni-directional	Low
Case 3	3	Uni-directional	High

As a final stage of all these classification stages, an accuracy assessment is performed by classification stability (CS) and best classification result (BCR) methods, apart from comparisons of level 1 visual interpretation results. CS explores differences in degrees of membership between the best and the second best class assignments of each object, which can give evidence about

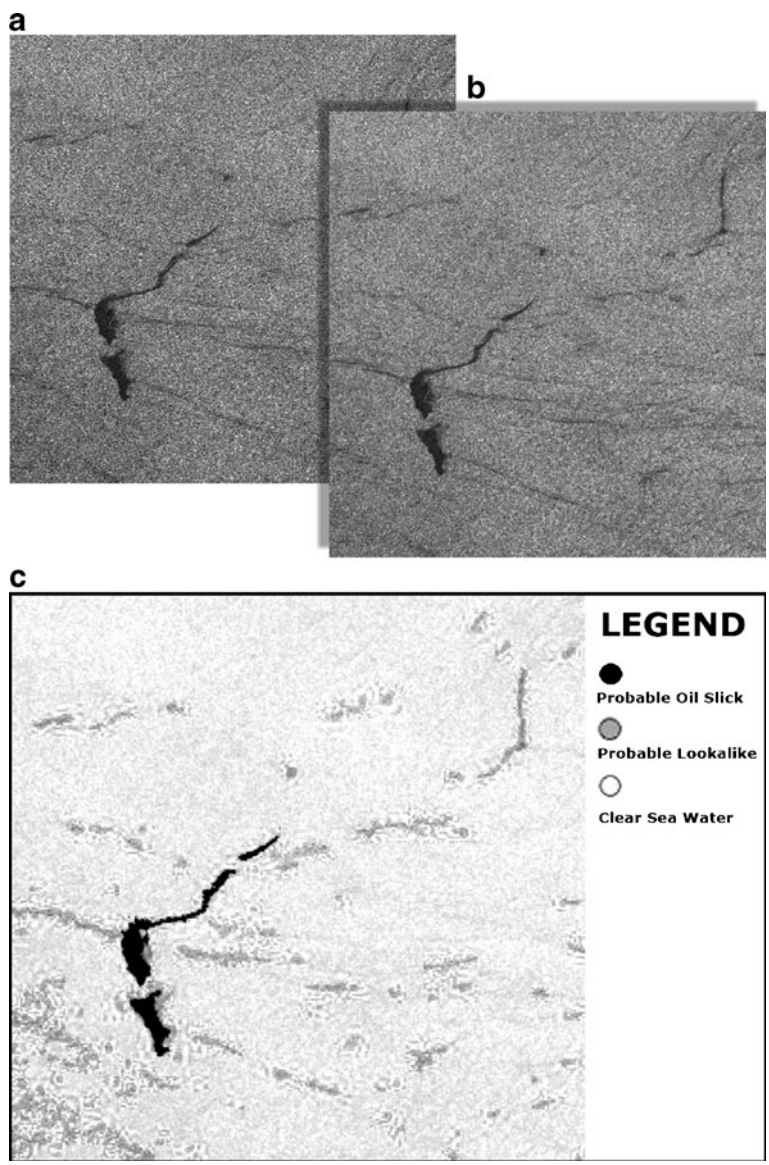

Fig. 3 **a** Example of case 1 subset image. **b** Opening morphology filter applied case 1 subset image. **c** Classified subset image sample scene for case 1 representing the discrimination of two dark spot classes

the ambiguity of an object's classification. On the other hand, BCR determines whether object has memberships in more than one class. In the accuracy assessment of classification schemes, basic statistical information describing the classes like number of image objects, mean, standard deviation, minimum value, and maximum value have been calculated.

Results

In the visual interpretation level, as the starting process, a second-order trend is removed from the images. Ten images from three different dates are manually interpreted, and 61 dark spots are detected. Based on these interpretations, 16 subset images are selected to be investigated in further stages. Throughout 16 subsets, 20 smaller scenes were selected and three different cases of dark spot occurrences were identified.

First case (case 1) is characterized by dark spots oriented in different direction and different contrast values. The second case (case 2) includes darks spots oriented in a single direction but having darker surroundings than the first case. The third case (case 3) contains dark spots isolated from the surroundings in homogeneity, contrast, and shape. As a result, six out of 20 scenes are categorized as "case 1," 11 as "case 2," and three as "case 3" (Table 2).

Case 1

First case includes dark spots with different orientations and different contrast with the surroundings (Fig. 3a). Firstly, noise removal filters are applied, and then radiometric resolution of the subset image is changed to 8 bit following the application of an opening morphological filter (Fig. 3b). For the segmentation of subset 1, a weight parameter of "2" is given to 8-bit morphology filter layer and "1" has been given to speckle filter layer. Segment scale parameter is decided as 20 after several trials. Shape factor is set to 0.4. Smoothness parameter is set to 0.7 yielding compactness to be automatically 0.3.

After segmenting the subset image, the specific features related to "layer values," "shape," and "texture" are automatically calculated for each segment. Sample segments are selected randomly, which are supposed to belong to one specific class. The interval of feature values is determined and tabulated (Table 3).

Based on the extracted features tabulated (Table 3), the membership functions are defined for the class hierarchy. For class "dark spot," a Boolean range membership function is defined using minimum pixel value morphologically filtered image. Since "probable oil slick" and "probable look-alike" classes are subclasses of "dark spot" class, this membership function appears to be an inherited function for them, and the rules are valid

Table 3 Features extracted from randomly selected sample segment representing ranges for membership boundaries of subset image sample scene for case 1

Features	Membership boundaries		
	Oil slick	Look-alike	Clear sea water
Mean layer value (8-bit morphology)	25–40	55–75	80–125
Mean layer value (filtered)	230–370	400–430	438–502
Brightness	180–210	230–260	257–315
Min. pixel value (8-bit morphology)	10–25	35–50	44–89
Max. pixel value (8-bit morphology)	50–60	90–155	146–89
Mean difference to neighbor pixels	(−32)–(−15)	(−42)–(−29)	(−12)–30
Mean difference to scene	(−132)–(−105)	(−62)–(−42)	(−34)–25
Area (meter square)	130–1,550	90–700	300–1,500
Length/width	1.5–6.6	1.9–4.7	1.2–1.7
Compactness	1.4–2.4	1.9–2.3	1.5–1.9
Shape index	1.5–2.9	1.4–2.5	1.1–2.2
Homogeneity	0.038–0.048	0.037–0.042	0.038–0.053
Contrast	860–1,280	1,170–1,405	1,050–1,350
Dissimilarity	20–27	25–29	24–27

Table 4 Features extracted from randomly selected sample segment representing ranges for membership boundaries of subset image sample scene for case 2

Features	Membership boundaries		
	Oil slick	Look-alike	Clear sea water
Mean layer value (8-bit morphology)	62–78	65–92	125–160
Mean layer value (filtered)	565–580	555–600	670–745
Brightness	305–330	310–347	345–450
Min. pixel value (8-bit morphology)	11–24	8–20	35–68
Max. pixel value (8-bit morphology)	105–129	113–143	175–225
Mean difference to neighbor pixels	(−50)–(−33)	(−20)–1	(−7)–(−1)
Mean difference to scene	(−95)–(−71)	(−93)–(−51)	25–90
Area (meter square)	300–2,300	500–1,900	300–1,400
Length/width	2.7–5.8	1–1.5	1.4–1.8
Compactness	2.4–4.7	1.7–2.3	2–3
Shape index	2.8–5.0	1.8–2.5	2.2–2.7
Homogeneity	0.033–0.047	0.040–0.047	0.043–0.048
Contrast	930–1,172	900–1,070	780–900
Dissimilarity	22–27	22–25	21–23

for the subclasses as well. The image is classified based on the membership functions, but some segments are found to be unclassified. In order to correct the unclassified areas, the membership function and logical operators are modified and tweaked for intersecting boundaries of feature values. Finally, the resultant classified image is obtained (Fig. 3c).

Finally, for the accuracy assessment, CS and BCR method is used to evaluate the accuracy of the classes. As a result of "classification stability," 39 segments out of 6,347 are classified as "probable oil slicks" with an accuracy of 90%, 213 segments are classified as "probable look-alikes" with an accuracy of 95%, and 6,095 segments are classified as "clear sea water" with an accuracy of 98%. Moreover, BCR showed that 99% of segments belonging to "probable oil slicks" has only one class; similarly, probability of segments belonging to "probable look-alikes" and "clear sea water" are 98% and 100%, respectively.

Case 2

All the processes that include image filtering and segmentation are repeated for the subsets

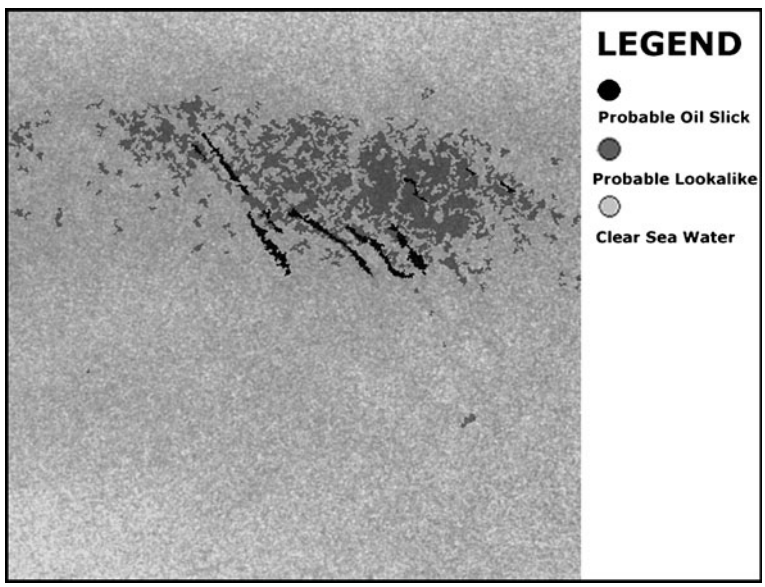

Fig. 4 Classified subset image sample scene for case 2 representing the discrimination of two dark spot classes

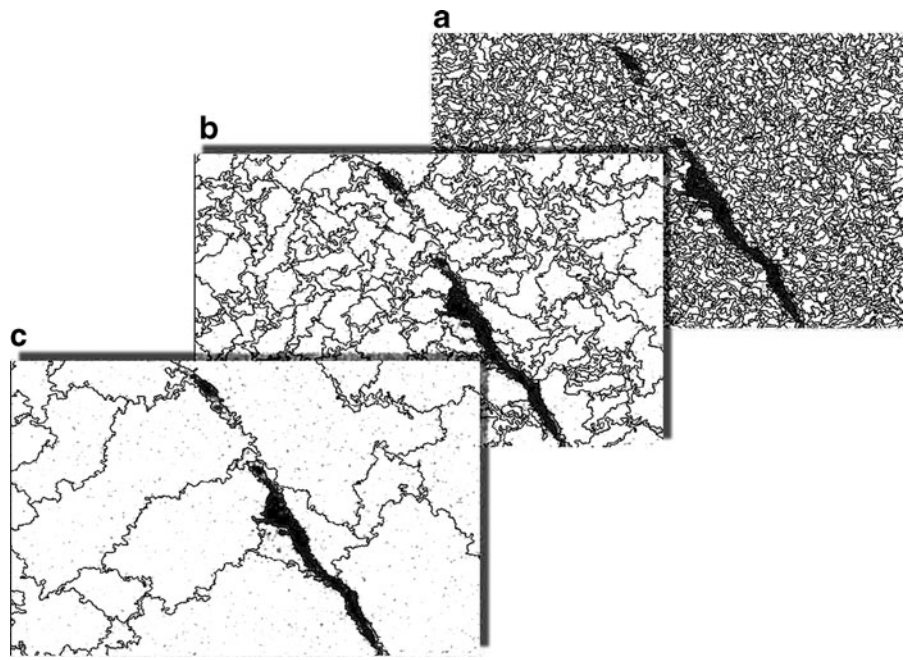

Fig. 5 Segmented subset image sample scene for case 3. **a** Scale parameter 20, **b** scale parameter 50, **c** scale parameter 100

of second case, Boolean range membership functions is defined based on boundaries presented on Table 4, and the image is classified (Fig. 4). When accuracy assessment of the classification by means of CS, it is found that 38 segments out of 6894 are classified as "probable oil slicks" with an accuracy of 65%, 420 segments are classified as "probable look-alikes" with an accuracy of 79%, and 6,436 segments are classified as "clear sea water" with an accuracy of 99%.

Case 3

The third case contains dark spots isolated from the surroundings in homogeneity, contrast, and shape. The difference of this case from previous cases is the abruptness of dark spot areas from the rest of the scene. Three different levels of segmentation are applied to the input images, and it is observed that increment in the scale factor provided identification of dark spots with single segments

Table 5 Features extracted from randomly selected sample segment representing ranges for membership boundaries of subset image sample scene for case 3

Features	Membership boundaries		
	Oil slick	Look-alike	Clear sea water
Mean layer value (8-bit morphology)	60–85	70–95	140–165
Mean layer value (filtered)	346–388	380–500	490–560
Brightness	205–235	230–310	315–370
Min. pixel value (8-bit morphology)	28–54	35–70	85–135
Max. pixel value (8-bit morphology)	92–119	105–143	170–225
Mean difference to neighbor pixels	(−61)–(−22)	(−20)–10	(−34)–39
Mean difference to scene	(−169)–(−143)	(−95)–(−49)	(−24)–41
Area (meter square)	265–1,171	300–560	450–900
Length/width	1.1–3.7	1.2–2.7	1.1–2.1
Compactness	2.1–2.4	1.5–2.5	1.7–2.6
Shape index	1.9–2.8	1.6–2.4	1.6–3.1
Homogeneity	0.024–0.040	0.038–0.042	0.026–0.036
Contrast	1,324–2,140	1,230–1,690	1,160–1,820
Dissimilarity	25–35	23–27	25–33

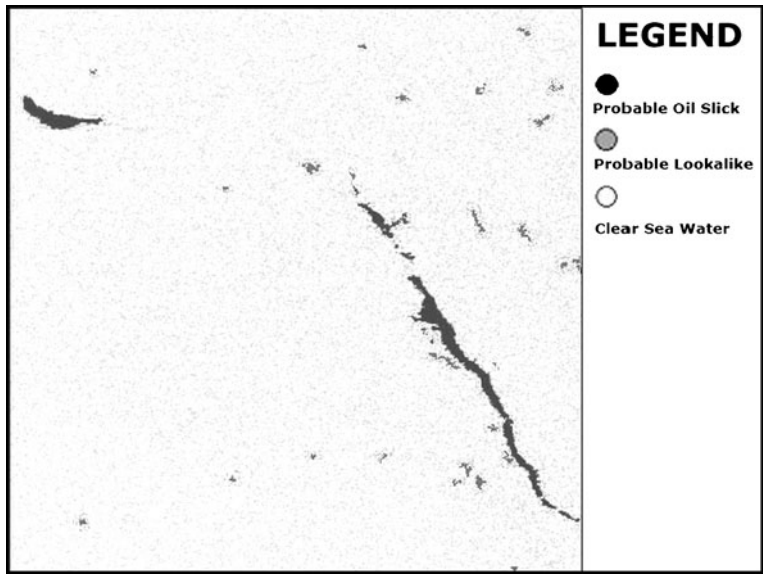

Fig. 6 Classified subset image sample scene for case 3 representing the discrimination of two dark spot classes

rather than multiple segments (Fig. 5). Smaller and more representative segments are created for dark spots whereas larger and more heterogeneous segments are created for lighter regions, which shadow dark spot information with small scale. This different levels of segmentation are another approach in object-based classification, and these three levels of segments are used in feature extraction stage. The segmentation is performed based on lower-scale parameter which is 20, and the other segmentation parameters kept the same as the previous cases. Then classification is done according to the membership boundaries represented in Table 5 and resulting image shown in Fig. 6.

The result of "classification stability" showed that 67 segments out of 7,601 are classified as "probable oil slicks" with an accuracy of 94%, 28 segments are classifies as "probable look-alikes" with an accuracy of 57%, and 7,506 segments are classified as "clear sea water" with an accuracy of 99%.

Discussion

First point of discussion is the classification method itself. Even if conventional pixel-based classification techniques are applied, instead of object-based methods, results would be less representative than the results of speckle and morphology filters because of substantial amount of noise. In addition, an adaptive pixel thresholding could also detect the dark areas from the lighter surroundings, but every single pixel having lower pixel value than the threshold is going to be defined as an oil slick, disregarding their neighborhood relations, which would lead to erroneous results. However, the applied methodology combines pixel-based filtering, supervision of human interpreter, object-based segmentation, and fuzzy classification. In object-based classification, the pixels are grouped to segments based on the two different input data. Membership functions helped to adjust the specific character of every individual subset. The algorithm converts every segment to a binary object with the help of Boolean range membership functions. The segments having the value of "1" for every membership function tied with "and" logical operator are assigned to one specific class.

Subset/case categorization is also a point of discussion. Every individual scene has its own feature character, and the membership boundaries should be re-evaluated. In every case, the weight or the impact of each extracted feature is different. For case 1, which has moderate contrast difference with the surroundings, features related to layer values and texture found to be more determinative than the shape-related features which are

important when the segment totally represents the dark spot area. They proved their importance in case 2, which has low contrast difference with the surroundings. Shape index, compactness, and length-to-width ratio features were found to be representative than the texture features. Area features directly related to size of the segments and therefore to the scale parameter. Increasing the scale parameter increases the segment area, and the segments containing whole dark spot can be classified using area values. However, in most of the cases, the dark spots are represented by multiple segments; thus, the impact of area feature has been found to be the least. Texture features like contrast homogeneity and dissimilarity, together with layer feature of "mean difference to scene," were the dominating features in class definitions of case 3, which has a major contrast difference with the surroundings. Consequently, for the impact weight of the feature, it can be said that layer values and texture values were more determinative for case 1 and case 3 whereas layer values and shape values were more discriminative in case 2.

The other point of discussion is the accuracy assessment which is the most important part of an image classification. In this respect, the classification accuracy is calculated from CS and BCR, in which they show the basic statistics and probability of segments belonging to the classes that they are assigned by the fuzzy logic defined by the membership functions. Since there is neither training set for class definition nor control set for absolute accuracy assessment, only the consistency of classes within themselves could be measured. However, it should be kept in mind that there is always a risk of obtaining wrong results even if class stability results show high level of consistency. Overall classification accuracy is calculated as averaging the results obtained from three cases. The calculated average classification accuracy (CS) for each class is found to be 83% for "probable oil slicks," 77% for "probable look-alikes," and 98.6% for "clear sea water." In order to focus on the main scope of the method, it is observed that the accuracy of classifying "probable oil slicks" decreases when the contrast difference of dark spots with the surroundings decreases. Case 2 is a good example of this situation. On the contrary, classification accuracy of "probable look-alikes" class decreases when contrast difference heterogeneity of the scene increases. Case 3 can be shown as an example of this situation.

The discrimination of man-made oil spills and the natural slicks are not considered throughout this study. There is always a probability of classified oil slicks to be originated from man-made structures like oil platforms or ships. These features appear as very bright spots in size of few pixels, and the dark spots in the near neighborhood can be in relation with them. Since there is not any known offshore oil platform in the region during the time of the images were acquired, the most common sources for man-made spills are the commercial ships. Major ship track ways can be used to optimize the false alarms for naturally originated slicks. However, in place of this information, temporal continuity can be checked, and it is more efficient in determining the source of the oil on the sea surface. If the oil is coming from a definite source at sea bottom, dark spots should be consistently present in a near neighborhood of pre-existing dark spot at different times. Location, orientation, and texture can be different from scene to scene based on the atmospheric conditions, weathering effect on the sea surface, and disruption within the water column. Throughout the 20 scenes of three different dates obtained from 16 subsets, 75% of the cases showed repetition in more than one image.

Conclusions

In this paper, an adapted system for detection of oil slicks in ENVISAT-ASAR images is presented. Major part of the oil slick detection problem is found to be to distinguishing oil slicks from other natural phenomena that create dark patches in the SAR image. The methodology worked satisfactorily in different cases of oil slicks, by combining different approaches. The discriminative power of human interpreter at the starting phase with the optimization of sea state conditions through speckle and morphology filters yielded a good basis for further segmentation steps. False classifications due to pixel-based approaches are minimized with the object-based

approach, and further discrimination between oil slicks and look-alikes became applicable through segmentation, fuzzy membership functions, and classification algorithms. The accuracy of classification is different for different cases of dark spots. For case 1, which has multiple orientation and moderate level of contrast to the surroundings, the obtained accuracy is 90%, 95%, and 98% for "probable oil slicks," "probable look-alikes," and "clear sea water" classes, respectively. For case 2, which has unique orientation and low level of contrast, the obtained accuracy is 65%, 79%, and 99% for "probable oil slicks," "probable look-alikes," and "clear sea water" classes, respectively. For case 3, which has unique orientation and high level of contrast to the surroundings, the obtained accuracy is 94%, 57%, and 99% for "probable oil slicks," "probable look-alikes," and "clear sea water" classes, respectively. The overall accuracy obtained by averaging three different cases is 83% for oil slicks and 77% for look-alikes.

Acknowledgements The authors would like to thank Turkish Petroleum Company (T.P.A.O) for provision of ENVISAT-ASAR images and hosting S. Akar during one of the offshore surveys in the study area.

References

Allan, T. D. (1983). *Satellite microwave remote sensing*. Chichester: Horwood, p. 526.

Arvelyna, Y., Oshima, M., Kristijuno, A., & Gunawan, I. (2001). Auto segmentation of oil slick in RADARSAT SAR image data around Rupat Island, Malaca Strait. In *22nd Asian conference on remote sensing*.

Baatz, M., & Schäpe, A. (2000). Multiresolution segmentation—an optimization approach for high quality multiscale image segmentation. In: J. Strobl, et al. (Eds.), *Angewandte Geographische Informationsverarbeitung XII* (pp. 12–23). Heidelberg: Wichmann.

Bertacca, M., Berizzi, F., & Mese, E. D. (2005). A FARIMA-based technique for oil slick and low-wind areas discrimination in sea SAR imagery. *IEEE Transactions On Geoscience And Remote Sensing, 43*(11), 2484–2493.

Brekke, C., & Solberg, A. H. S. (2005). Oil spill detection by satellite remote sensing. *Remote Sensing of Environment, 95*, 1–13.

Clarke, R. H., & Cleverly, R. W. (1991). Petroleum seepage and post-accumulation migration. In: W. A. England, J. A. Fleet (Eds.), *Petroleum migration* (pp. 265–271). London: Geological Society.

Dalling, P. S., & Strøm, T. (1999). Weathering of oils at sea: model/field data comparisons. *Spill Science & Technology Bulletin, 5*(1), 63–74.

eCognition. (2004). *User guide*. München: Definiens Imaging, p. 486.

Ergün, M., Dondurur, D., & Çiftçi, G. (2002). Acoustic evidence for shallow gas accumulations in the sediments of the Eastern Black Sea. *Terra Nova, 14*(5), 313–320.

Espedal, H. A., & Wahl, T. (1999). Satellite SAR oil spill detection using wind history information. *International Journal of Remote Sensing, 20*(1), 49–65.

Fingas, M. F., & Brown, C. E. (1997). Review of oil spill remote sensing. *Spill Science &Technology Bulletin, 4*(4), 199–208.

Fiscella, B., Giancaspro, A., Nirchio, F., Pavase, P., & Trivero, P. (2000). Oil spill detection using marine SAR images. *International Journal of Remote Sensing, 21*(18), 3561–3566.

Friedman, K. S., Pitchel, W. G., Clemente-Colon, P., & Li, X. (2002). GoMEx—an experimental GIS system for the Gulf of Mexico Region using SAR and additional satellite and ancillary data. In *International Geoscience and Remote Sensing Symposium, IGARSS '02, 6*, pp. 3343–3345.

Girard-Ardhuin, F., Mercier, G., & Garello, R. (2003). Oil slick detection by SAR imagery: Potential and limitation. In *Proc. OCEANS 2003, 1*, pp 164–169.

Girard-Ardhuin, F., Mercier, G., Collard, F., & Garello, R. (2005). Operational oil-slick characterization by SAR imagery and synergistic data. *IEEE Journal of Oceanic Engineering, 30*(3), 487–495.

Gonzalez, R. C. , & Richards, E. W. (1992). *Digital image processing*. Reading: Addison-Wesley, p. 716.

Greinert, J., Artemov, Y., Egorov, V., De Batist, M., & McGinnis, D. (2006). 1300-m-high rising bubbles from mud volcanoes at 2080m in the Black Sea: Hydroacoustic characteristics and temporal variability. *Earth and Planetary Science Letters, 244*, 1–15.

Haralick, R. M. , Shanmugan, K., & Dinstein, I. (1973). Textural features for image classification. *IEEE Transactions on Systems, Man and Cybernetics, SMC-3*(6), 610–621.

Hofmann, T., Pizucha, J., & Buchman, J. (1998). Unsupervised texture segmentation in a deterministic annealing framework. *IEEE Transactions on Pattern nalysis and Machine Intelligence, 20*(8), 803–818.

Hovland, H. A., Johannessen, J. A., & Digranes, G. (1994). Slick detection in SAR images. In *Proc. IGARSS'94*, 4, pp. 2038–2040.

Huang, B., Li, H., & Huang, X. (2005). A level set method for oil slick segmentation in SAR images. *International Journal of Remote Sensing, 26*(6), 1145–1156.

Karantzalos, K., & Argialas, D. (2008). Automatic detection and tracking of oil spills in SAR imagery with level set segmentation. *International Journal of Remote Sensing, 29*(21), 6281–6296.

Karathanassi, V., Topouzelis, K., Pavlakis, P., & Rokos, D. (2006). An object-oriented methodology to detect oil

spills. *International Journal of Remote Sensing, 27*(23), 5235–5251.

Keramitsoglou, I., Cartalis, C., & Kiranoudis, C. T. (2006). Automatic identification of oil spills on satellite images. *Environmental Modelling & Software, 21*, 640–652.

Leifer, I., Luyendyk, B., & Broderick, K. (2006). Tracking an oil slick from multiple natural sources, Coal Oil Point, California. *Marine and Petroleum Geology, 23*, 621–630.

Li, F., & Shen, C. (2010). A two-stage method for oil slick segmentation. *International Journal of Remote Sensing, 31*(15), 4217–4226

Lombardo, P., & Oliver, C. J. (2000). Optimum detection and segmentation of oil-slicks using polarimetric SAR data. *IEE Proc.-Radar, Sonar Navigation, 147*(6), 309–321.

Macdonald, R., Leifer, I., Sassen, R., Stine, P., Mitchell, R., & Guinasso, J. R. (2002). Transfer of hydrocarbons from natural seeps to the water column and atmosphere. *Geofluids, 2*, 95–107.

Mao, J., & Jain, A. (1992). Texture classification and segmentation using multiresolution simultaneous autoregressive models. *Pattern Recognition, 25*, 173–188.

Meinel, G., & Neubert, M. (2004). A comparison of segmentation programs for high resolution remote sensing data. In *Proceedings of the ISRPS 2004 annual conference, Istanbul, Turkey*, pp. 19–23.

Mouche, A. A., Hauser, D., Daloze, J., & Guerin, C. (2005). Dual-polarization measurements at C-Band over the ocean: Results from airborne radar observations and comparison with ENVISAT ASAR data. *IEEE Transactions On Geoscience and Remote Sensing, 43*(4).

Nirchio, F., Sorgente, M., Giancaspro, A., Bianmino, W., Parisato, E., Ravera, R., et al. (2005). Automatic detection of oil spills from SAR images. *International Journal of Remote Sensing, 26*(6), 1157–1174.

O'Brein, G. W., Lawrence, G. M., Williams, A. K., Glenn, K., Barrett, A. G., Lech, M., et al. (2005). Yampi Shelf, Browse Basin, North-West Shelf, Australia: A test-bed for constraining hydrocarbon migration and seepage rates using combinations of 2D and 3D seismic data and multiple, independent remote sensing technologies. *Marine and Petroleum Geology, 22*, 517–549.

Okay, A. I., Şengör, A. M. C., & Görür, N. (1994). Kinematic history of the opening of the Black Sea and its effect on the surrounding regions. *Geology, 22*, 267–270.

Pellemans, A. H. J. M., Bos, W. G., Konnings, H., & Van Swol, R. W. (1995). Oil spill detection on the North Sea using ERS-1 SAR data. *Beleids Commisie Remote Sensing, BCRS report*, pp. 94–30.

Roberts, D. G. (1998). Regional and petroleum geology of the Black Sea and surrounding region. *Marine and Petroleum Geology, 15*(4), 381–383.

Robinson, A. G., Rudat, J. H., Banks, C. J., & Wiles, R. L. F. (1996). Petroleum geology of the Black Sea. *Marine and Petroleum Geology, 13*(2), 195–223.

Rollet, N., Logan, G. A., Kennard, J. M., O'Brein, P. E., Jones, A. T., & Sexton, M. (2006). Characterisation and correlation of active hydrocarbon seepage using geophysical data sets: An example from the tropical, carbonate Yampi Shelf, Northwest Australia. *Marine and Petroleum Geology, 23*, 145–164.

Rudorff, F. M., & Gherardi, D. F. M. (2008). Coral reef detection using SAR/RADARSAT-1 images at Costa dos Corais, PE/AL, Brazil. *Brazilian Journal of Oceanography, 56*(2), 85–96.

Russ, J. C. (1992). *The image processing handbook*. Boca Raton: CRC, p. 445.

Ryerson, R. A. (1998). *Manual of remote sensing: Imaging radar, vol. 2*. New York: American Society for Photogrammetry and Remote Sensing, Wiley.

Shu, Y., Li, J., Yousif, H., & Gomeset, G. (2010). Dark-spot detection from SAR intensity imagery with spatial density thresholding for oil-spill monitoring. *Remote Sensing of Environment, 114*, 2026–2035.

Smith, A. J. E., & Melger, F. J. (2003). Using the cross-spectral phase to filter slicks in the ENVISAT ASAR wave mode product. *International Journal of Remote Sensing, 24*(24), 5391–5396.

Solberg, A. H. S., Storvik, G., Solberg, R., & Volden, E. (1999). Automatic detection of oil spills in ERS SAR images. *IEEE Transactions on Geoscience and Remote Sensing, 37*(4), 1916–1924.

Solberg, A. H. S., Brekke, C., & Husøy, P. O. (2007). Oil spill detection in Radarsat and Envisat SAR images. *IEEE Transactions on Geoscience and Remote Sensing, 45*(3), 746–755.

Topouzelis, K. N. (2008). Oil spill detection by SAR images: Dark formation detection, feature extraction and classification algorithms. *Sensors, 8*, 6642–6659.

Wackerman, C. C. (1992). Digital SAR image formation. In F. D. Carsey (Ed.), *Microwave remote sensing if sea ice. Geophysical monograph 68* (pp. 105–110). Washington, DC: AGU.

Williams, A., & Lawrence, G. (2002). The role of satellite seep detection in exploring the South Atlantic's ultradeep water. In D. Schumacher, L. A. LeSchack (Eds.), *Surface exploration case histories: Applications of geochemistry, magnetics, and remote sensing. AAPG Studies in Geology No. 48 and SEG Geophysical References Series No. 11* (pp. 327–344). Boulder: AAPG.